Amplitude and phase retrieval in simultaneous $\pi/2$ phase-shifting heterodyne interferometry using the synchrosqueezing transform

Arturo Bianchetti,[1,*] Francisco E. Veiras,[1,2] Pablo Etchepareborda,[1] Ana Laura Vadnjal,[1] Alejandro Federico,[1] and Guillermo H. Kaufmann[3]

[1]Electrónica e Informática, Instituto Nacional de Tecnología Industrial,
P.O. Box B1650WAB, B1650KNA San Martín, Argentina

[2]Laboratorio de Sistemas Líquidos, GLOmAe, Departamento de Física, Facultad de Ingeniería,
Universidad de Buenos Aires, Avenida Paseo Colón 850,
Ciudad Autónoma de Buenos Aires, C1063ACV, Argentina

[3]Instituto de Física Rosario (CONICET-UNR) and Centro Internacional Franco
Argentino de Ciencias de la Información y de Sistemas (CONICET-UNR-AMU),
Ocampo y Esmeralda, S2000EZP Rosario, Argentina

*Corresponding author: arturob@inti.gov.ar

This paper presents a method for amplitude and phase retrieval in simultaneous $\pi/2$ phase-shifting heterodyne interferometry. The used optical setup admits the introduction of a temporal carrier and simultaneously verifies the two-beam interferometry equation for each intensity signal, which are $\pi/2$ rad out of phase (quadrature). The spatiotemporal recovering process is obtained by isolating the object amplitude and phase using wavelet transform analysis of the temporal series composed by the difference between the measured pixel intensities corresponding to each quadrature signal. This process is subsequently improved by introducing a framework based on the synchrosqueezing transform, which recovers the data of interest with higher accuracy when very low scattering amplitudes and phase excursions must be determined in noisy working conditions. The advantages and limitations of the presented method are analyzed and discussed using numerical simulations and also experimental data obtained from temporal speckle pattern interferometry.   © 2015 Optical Society of America

OCIS codes: (100.2000) Digital image processing; (100.5070) Phase retrieval; (120.3180) Interferometry; (120.5050) Phase measurement; (120.6150) Speckle imaging.

http://dx.doi.org/10.1364/AO.54.002132

1. Introduction

When inspecting and evaluating microelectromechanical systems, full-field and noninvasive optical techniques are desirable to get access to spatially resolved properties and parameters of materials because they do not alter the integrity and mechanical behavior. In addition, since the surface profile, deflection, motion, and vibration amplitude of microsystems are typically in the range of nanometers to a few microns, interferometry-based evaluation methods are of primary interest [1]. This approach is widely benefitted when sophisticated signal and image processing techniques also are used. The processing techniques also can help to deliver detailed information on the local structure and dynamics of the analyzed microsystem.

The heterodyne interferometry technique (HI) is a good alternative to use in optical characterization of a wide range of transient physical parameters produced by diffusely reflecting objects. In the application of this technique, the dynamics of the object under test produces intensity fluctuations at all pixels belonging to the recorded time series of interferograms. The sequential acquisition of a large number of interferograms and its digital post-processing facilitate the optical phase retrieval by using a point-by-point analytical phase-shifting algorithm along the temporal axis. Therefore, the adopted phase unwrapping procedure involves one-dimensional (1D) analysis and avoids the implementation of two- and three-dimensional (2D and 3D) complex spatiotemporal unwrapping methods, minimizing the recovered object phase errors.

The weakness of the HI method is its low tolerance to unwanted effects such as nonmodulated pixels, modulation loss and noise, which make the retrieval process difficult. To reduce the influence of these drawbacks, HI is improved with the assistance of robust object amplitude and phase retrieval frameworks, which are designed using digital signal and image processing algorithms. Particularly, in digital speckle pattern interferometry and related techniques [2], the application of signal and image processing methods using the continuous wavelet transform analysis has received lot of attention in the last two decades. Moreover, its application in the phase computation problem has been extensively documented since the mid-1990s [3]. In addition, readers interested in the development of speckle and related techniques for the inspection and evaluation of microelectromechanical systems can read Chap. 15 in [1]. It is important to know that the common application of the speckle interferometric techniques for experimental mechanics application are in the order of 10 nm of displacement resolution [4].

In the wavelet transform analysis of two-beam interferometric signals, an external operator must fix several parameters of the algorithm to counteract the influence of background intensity and improve the time-scale representation, and to obtain better readability of the instantaneous amplitude and phase produced by the object under test. These tasks are time-consuming and can be difficult to solve when low object phase excursions and scattering amplitudes must be determined in noisy measurement conditions. This drawback is even more severe when temporal speckle pattern interferometric signals are present during the acquisition.

To tackle these major flaws, we present a method for spatiotemporal amplitude and phase recovering using an optical arrangement composed by a simultaneous $\pi/2$ phase-shifting heterodyne interferometer, assisted with the synchrosqueezing transform framework for high improvement of the wavelet transform analysis of the interferometric measurements.

The optical setup we used is based on a Twyman–Green interferometer, which can simultaneously give two interferograms of $\pi/2$ rad out of phase. An analogous optical setup was used for nanoparticle detection in [5], although a phase recovery procedure was not implemented. As each interferogram verifies the well-known two-beam interferometry equation, the working signal is defined by the difference of both interferograms and then removes the influence of background intensity. Therefore, this signal is the main one we will analyze for the instantaneous local amplitude and phase retrieval process.

With the external introduction of a temporal carrier in the optical setup, the instantaneous frequency of this difference signal is carrier-frequency shifted in its time-scale wavelet analysis representation. Consequently, the technique of ridge extraction procedure is improved and better accuracy in the instantaneous amplitude and phase retrieval is obtained. However, we can still obtain high-quality time-frequency representations by introducing the synchrosqueezing transform framework. Synchrosqueezing is an adaptive and invertible transform developed to enhance the quality of the wavelet-based analysis. With the introduction of this framework, the amplitude of the scattered field and the instantaneous phase corresponding to the object under test can be determined more accurately than with the common implementations of the wavelet transform analysis previously described. This approach generates a more robust spatiotemporal amplitude and phase recovery method with a less laborious intervention of the operator when micro and nano out-of-plane displacement fields must be determined in microsystems subject to noisy measurement conditions.

2. Simultaneous $\pi/2$ Phase-shifting Heterodyne Interferometer

By introducing polarized light in a Twyman–Green interferometer, we can obtain multiple simultaneous interferograms with different values of the constant phase difference by selecting the phase through the orientation of a properly positioned analyzer. There are several techniques for simultaneously obtaining two interferograms with $\pi/2$ rad out of phase [6]. In this work, we use the optical setup shown in Fig. 1 for out-of-plane displacement field measurements in microsystems. The laser output ($\lambda = 532$ nm) is linearly polarized at an angle of $\alpha = 45°$ with respect to the coordinate system (x, y) by using a polarizer (P1). A nonpolarized beam splitter (NPBS) reflects a part of the incident light to the reference arm and transmits the other part to the test arm. A $\lambda/4$ wave plate (QWP) and subsequently other polarizer (P2) are placed in the reference arm, oriented along the x axis at $\alpha = 45°$ and $\alpha = 0°$, respectively. This combination (QWP + P2) sets the reference signal polarization to be circular. NPBS combines the light coming from both arms and sends it to a polarizing beam splitter (PBS). This last component discriminates the two
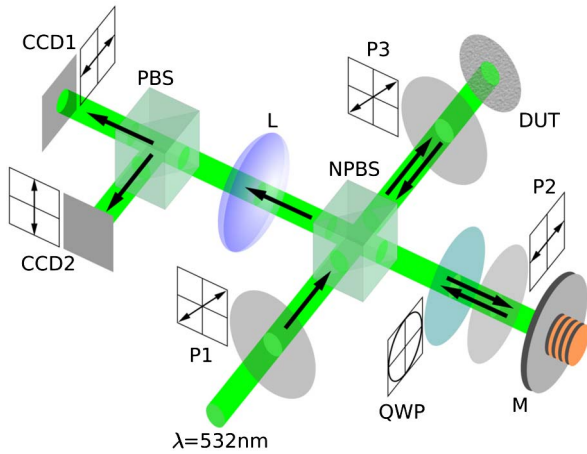
Fig. 1. Simultaneous $\pi/2$ phase-shifting heterodyne interferometer used in spatiotemporal amplitude and phase retrieval. CCD1 and CCD2 are detectors; PBS and NPBS are polarized and nonpolarized beam splitters, respectively; QWP is the $\lambda/4$ wave plate; DUT is the device under test; M is a piezo-electrically driven mirror; P1, P2, and P3 are polarizers; and L is the lens of focal length f. Arrows and x–y diagrams indicate beam propagation directions and polarization states, respectively.

orthogonal polarization states that are registered separately in two CCD detectors (CCD1 and CCD2), obtaining a difference in relative phase between both detections of $\pi/2$ rad.

We introduced the temporal carrier using the reference mirror (M), which is piezoelectrically driven. The light that travels along the test arm is reflected on the device under test (DUT). To ensure linear polarization after reflection, a polarizer (P3) with its transmission axis parallel to the polarization plane of the incoming light is interposed. Therefore, the superposition of light coming from these two branches, one with linear polarization and the other with circular polarization is composed by two intensity signals with phase difference of $\pi/2$ rad and orthogonal polarizations.

The output of this optical setup consists of two frequency-shifted intensity signals that verify the two-beam interferometry equation and are $\pi/2$ rad out of phase. By denoting $E_s(t)$ and $E_r(t)$ as the object scattering and reference fields, respectively, the output intensities $I_1(t)$ and $I_2(t)$ at each corresponding CCD detector can be characterized by the following expressions:

$$I_1(t) = I_B(t) + I_M(t)\cos[\phi(t)]$$
$$I_2(t) = I_B(t) + I_M(t)\sin[\phi(t)], \qquad (1)$$

where $I_B(t) \equiv |E_r(t)|^2 + |E_s(t)|^2$ is the background intensity, $I_M(t) \equiv 2|E_r(t)||E_s(t)|$ is the modulation intensity, $\phi(t)$ is the temporal phase difference between the object $\phi_o(t)$, and reference $\phi_r(t)$ phases. In this equation, the spatial coordinates and initial phases are omitted for clarity.

It is simple to show that the signal difference

$$\Delta I(t) \equiv I_1(t) - I_2(t) \quad \text{and}$$
$$\Delta I(t) = \sqrt{2}I_M(t)\cos[\phi(t) + \pi/4], \qquad (2)$$

does not contain the term corresponding to the background intensity when it is compared with the two-beam interferometry equation.

In the following section, we briefly discuss the wavelet transform analysis of $\Delta I(t)$ and emphasize the improvement obtained in the time-frequency wavelet representation by adopting the synchrosqueezing transform framework.

3. Theoretical Description

A. Wavelet Transform Analysis

In the wavelet transform analysis for instantaneous amplitude and phase retrieval, the selection of $\Delta I(t)$ as the working signal is a better choice than the usual procedure of selecting the interferometric intensity ($I_1(t)$ or $I_2(t)$) analysis and also to implement external filtering methods for high signal reconditioning to avoid the influence of $I_B(t)$. Furthermore, the selection of a proper analytical wavelet and the introduction of a temporal carrier in the optical setup can also be insufficient when very low instantaneous amplitude and phase values must be determined in noisy measurement conditions. Discussions about the influence of the different parameters involved in the wavelet transform analysis are well documented in the specialized literature, and interested readers could read [3] for specific details in the phase recovery procedures when the two-beam interferometry technique is implemented.

Using proper working conditions and the optical setup described in Fig. 1, we can consider $\Delta I(t)$ as an asymptotic and locally monochromatic signal, where the instantaneous amplitude $A(t) = \sqrt{2}I_M(t)$ and the phase $\phi(t)$ verify $|\partial\phi(t)/\partial t| \gg |A(t)^{-1}\partial A(t)/\partial t|$. Therefore, by means of the Hilbert transform, it is possible to obtain an analytic signal close to the exponential model $z(t) = A(t)\exp[i\phi(t)]$. The purpose of using this analytic signal is to improve the time-scale representation in a wavelet decomposition approach.

Remember that a wavelet function is a square-integrable complex-valued function $\psi(t)$ with a zero average centered in the neighborhood of $t = 0$. The time-scale representation is carried out by scaling ψ by $a \in \mathbb{R}_{>0}$ and by translating it by $b \in \mathbb{R}$ (with $\mathbb{R}$ the set of real numbers). The continuous wavelet transform $W_z(a, b) = a^{-1/2} \int_{\mathbb{R}} dt\psi^*[a^{-1}(t-b)]z(t)$ decomposes the working signal $z(t)$ over dilated and translated wavelets; ($*$) denotes complex conjugation. Note that $W_z(a, b)$ computes the fluctuations of the signal $z(t)$ around the point b at the scale given by a. This time-scale wavelet representation involves the use of a wide range of scales for the analysis of $z(t)$ in a so called "multiresolution analysis."

To measure the time evolution of frequency transients in $z(t)$, we propose the use of a complex analytic

wavelet that separates the amplitude and the phase components, this being the Morlet wavelet $\psi(t) = \pi^{-1/4}[\exp(i\omega_0 t) - \exp(-\omega_0^2/2)]\exp(-t^2/2)$, with $\omega_0 \in \mathbb{R}$. In practice, the carrier frequency is known and the ridge extraction is usually performed by tracking the local maximum at $t = b$. Then, the instantaneous amplitude and phase of the analyzed signal can be determined without ambiguity.

The wavelet transform analysis is applied to extract the instantaneous amplitude and phase of the signal $z(t)$ by detecting the ridge of the obtained wavelet transform. Note that the instantaneous amplitude $A(t)$ is related with the scattering field amplitude $|E_s(t)|$, which amplifies by more than twice the reference field amplitude $|E_r(t)|$ compared with the common use of two-beam interferometry in out-of-plane measurements as shown in Eq. (2). Although this amplification feature is an advantage when low amplitudes of the scattering field must be determined, the wavelet transform also can yield blurred time-scale representations. Therefore, the method's accuracy is reduced for instantaneous characterizations in noisy measurement conditions. The next section addresses this problem in detail.

B. Synchrosqueezing Transform Analysis

The dynamics of the out-of-plane displacements of the object under test produces fluctuating intensity signals commonly termed nonstationary signals. Several time-frequency methods have been proposed to address this problem. In [3], some inherent limitations of these methods are discussed for two-beam interferometry. Note that the obtained values are spread over the time-frequency representations where the geometry depends jointly on the analyzed signal, the employed analyzing windows, and the wavelet functions. Note also that the Heisenberg uncertainty principle introduces a severe limit in the resolution attained in the time-frequency representation. Therefore, different compromises are achievable by the selection of the transform and the set of the basis functions used in the decomposition. To overcome these difficulties, a significant improvement is obtained by introducing the time-frequency reassignment and synchrosqueezing techniques [7].

In this work, we used the synchrosqueezing framework [8], which can be viewed as a special case of the reassignment approach [7]. Reassignment techniques aim to sharpen the time-frequency representation $\mathcal{R}(t, \omega)$ by allocating its value to a different point (t', ω') in the time-frequency plane, determined by the local behavior of $\mathcal{R}(t', \omega')$ around (t, ω). In the case of synchrosqueezing, once the $W_z(a, b)$ is computed for any (a, b) with $W_z(a, b) \neq 0$, the instantaneous frequency estimate $\omega_z(a, b)$ is defined as

$$\omega_z(a, b) = \frac{-i}{W_z(a, b)}\frac{\partial}{\partial b}W_z(a, b), \qquad (3)$$

and, by means of this relation, the information from the time-scale plane to the time-frequency plane is transferred according to the reassignment map $(a, b) \mapsto [\omega_z(a, b), b]$. Note that $W_z(a, b)$ is computed at discrete values a_k, $k \in \mathbb{N}$ (with $\mathbb{N}$ the set of natural numbers). Assuming a linear scale discretization of ω and following [8], the synchrosqueezed transform $T_z(\omega_l, b)$ is obtained by adding the different contributions

$$T_z(\omega_l, b) = \Delta\omega^{-1}\sum_{\mathcal{D}}W_z(a_k, b)a_k^{-3/2}(\Delta a)_k, \qquad (4)$$

where $\mathcal{D} = \{a_k : |\omega(a_k, b) - \omega_l| \leq \Delta\omega/2\}$ with $(\Delta a)_k \equiv {}_ak - a_{k-1}$, and ω_l are the centers of the successive bins $[\omega_l - \Delta\omega/2, \omega_l + \Delta\omega/2]$ for $\Delta\omega \equiv \omega_l - \omega_{l-1}$. In this piecewise constant approximation, the signal $z(t)$ is finally recovered by means of the following relation:

$$z(b) = \mathcal{C}\sum_{l \in \mathcal{L}}T_z(\omega_l, b), \qquad (5)$$

where $\mathcal{C}$ is a given normalization constant, and $\mathcal{L}$ is the set composed by indices $\{l_1, l_2, ...\}$ that denotes a given frequency band in the reassignment time-frequency map. This family of indices can be selected by an external operator or can follow a given computational procedure. From Eq. (5), the instantaneous object scattering amplitude and phase are obtained by simple algebra: $|E_s(b)| = A(b)/[2\sqrt{2}|E_r(b)|]$ and $\phi_o(b) = \phi(b) + \phi_r(b)$, respectively. Figure 2 shows a conceptual block diagram and summarizes the main stages of the instantaneous amplitude and phase retrieval process.

The synchrosqueezing transform algorithm is implemented using the discretization of Eqs. (3–5), a process that requires dedication. An efficient numerical implementation with complete discussions on several issues present in this process is shown in [9]. The practical setting of various parameters also is presented. In addition, a toolbox composed by MATLAB scripts is offered via a web link for reproducibility purposes.
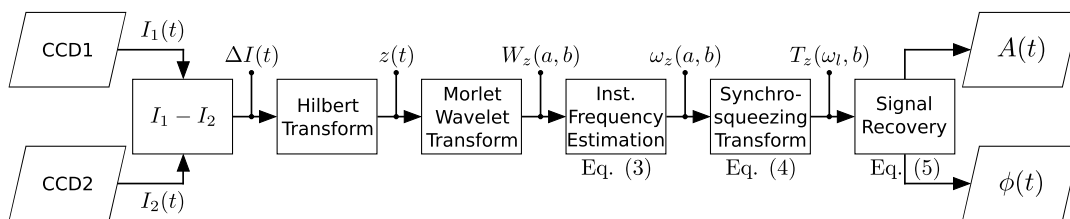

Fig. 2. Conceptual block diagram for the proposed instantaneous amplitude $A(t)$ and phase $\phi(t)$ retrieval method. Labels Eq. (3), Eq. (4), and Eq. (5) correspond to the main stages of the synchrosqueezing wavelet transform implementation.

4. Numerical Results

To illustrate the performance of the phase recovery procedure, we analyzed simulated temporal speckle pattern interferometry signals produced by the simultaneous $\pi/2$ phase-shifting heterodyne interferometer described in Fig. 1. We began the numerical analysis by introducing a temporal carrier of frequency $f_c = 220$ and by generating interferograms having an average speckle size $s = 2$ pixels following the procedure described in [10]. Numerical speckles were computed using a linear amplitude image model. The speckle amplitude was obtained by means of an integral convolution between a diffuser and the impulse response of a $4f$ optical system. The diffuser is assumed to be a pure phase object with phase excursions uniformly distributed over $(-\pi, \pi]$. Two characteristic signals represented by the intensities $I_1(n_x, n_y, t_n)$ and $I_2(n_x, n_y, t_n)$ are obtained at specific pixels (n_x, n_y) with $1 \leq n_x, n_y \leq 128$ at spaced-out time intervals $t_n \in [0, 1]$, $1 \leq n \leq 1536$ frames, for the CCD1 and the CCD2 detectors, respectively.

The phase corresponding to the simulated dynamic out-of-plane displacement field $z(n_x, n_y, t_n)$ is selected in accordance with the temporal-spatial product function $\phi_E(n_x, n_y, t_n) = \phi_s(n_x, n_y)\phi_t(t_n)$, where the temporal function $\phi_t(t_n)$ is represented in Fig. 3 and the spatial function is given by the identity $\phi_s(n_x, n_y) = \exp[-8(x^2 + y^2)]$ for linear scaling functions $\{x, y\} = \{x(x_n); y(y_n)\} \in [-1, 1]$ centered in pixel coordinates $n_x = 64$, $n_y = 64$. Note that the temporal-spatial phase distribution can be seen as a Gaussian spatial function temporally modulated that changes its deformation state following different concavity values. Also note that the out-of-plane displacement components are related with the phase change $\Delta\phi$ by means of the identity $z(n_x, n_y, t_n) = \lambda\Delta\phi(n_x, n_y, t_n)/4\pi$, where λ is the wavelength of the laser [2].

In this numerical analysis, we considered that the carrier amplitude is three orders of magnitude higher than the corresponding object amplitude (i. e. $|E_s| = \alpha|E_r|$, with $\alpha = 0.001$). To simulate the modulation loss and noise, four independent random
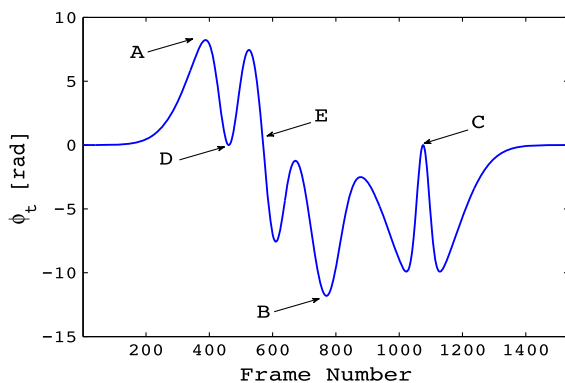
variables were introduced in the numerical model. Two random variables with uniform distribution in $[-\pi/20, \pi/20]$ are added to the object and carrier phase generation in each temporal frame. Likewise, the other two random variables with normal distributions and standard deviations $\sigma_1 = 10^{-1}$ and $\sigma_2 = 10^{-4}$ are added to the carrier and object amplitudes, respectively. Finally, the obtained interference signals are discretized by using a 14-bit scale.

The performance obtained by the proposed approach is illustrated first by means of the analysis of the simulated interferometric signals at the central pixel $n_x = 64$, $n_y = 64$. For this purpose, the corresponding scalograms $|W_z(a, b)|$ and its reassignment $|T_z(\omega, b)|$ are computed using the Morlet wavelet with the parameter $\omega_0 = 2\pi$ and 1024 scales. Figure 4(a) shows the scalogram $|W_z(a, b)|$ that corresponds to the wavelet analysis of the interferometric signal $I_1(64, 64, t_n)$ when its dc component is removed. Note that this situation is equivalent to recover the object phase with the usual procedure by using an common out-of-plane interferometer and the two-beam interferometry equation. In this figure, the wavelet phase recovery method fails due to the high level noise involved in the measurement system. Consequently, it is impossible to identify the significant ridges by tracking the set of the local maxima. However, using the simultaneous $\pi/2$ phase-shifting heterodyne interferometer, a differential working condition was applied and then the scalogram $|W_z(a, b)|$ obtained for the signal difference $\Delta I(64, 64, t_n)$ is clearly improved, as shown in Fig. 4(b). Nevertheless, this representation was still too vague to obtain good results and consequently the application of the ridge extraction procedure failed. To overcome this limitation, the synchrosqueezing algorithm was applied to obtain a clearer time-scale representation.

This process $|T_z(\omega, b)|$ is obtained from $W_z(a, b)$ following Eqs. (3) and (4) for the difference signal analysis. Figure 4(c) shows the corresponding sharpened result with the consequent improvement. Then, by applying the synchrosqueezing transform, the tracking of the local maxima can be easily carried out using a common computational routine. Note the improvement of the ridge detection obtained in the neighborhood of the points D (local minimum), E (zero crossing), and C (local maximum) shown in Fig. 3, with medium, slow, and high instantaneous frequency variations, respectively. As usual, the phase distribution is retrieved using the arctan equation and a conventional 1D unwrapping method along the time axis by excluding robust procedures of 2D phase unwrapping [3].

Figure 5 depicts the obtained out-of-plane displacement components between the frames labeled $A(t_{388})$ and $C(t_{1076})$, and $B(t_{770})$ and $C(t_{1076})$ shown in Fig. 3. Figures 5(a) and 5(c) show the original displacement components corresponding to $\Delta\phi_{AC} = \phi(A) - \phi(C)$ and $\Delta\phi_{BC} = \phi(B) - \phi(C)$, respectively. Figures 5(b) and 5(d) show the determined displacement field for the recovered phase differences $\Delta\phi_{AC}$ and $\Delta\phi_{BC}$,

Fig. 3. Temporal function associated with the simulated spatial–temporal phase excursion. A, B, and C are reference points for the phase difference calculation in Fig. 5. C, D and E are points of null phase values.
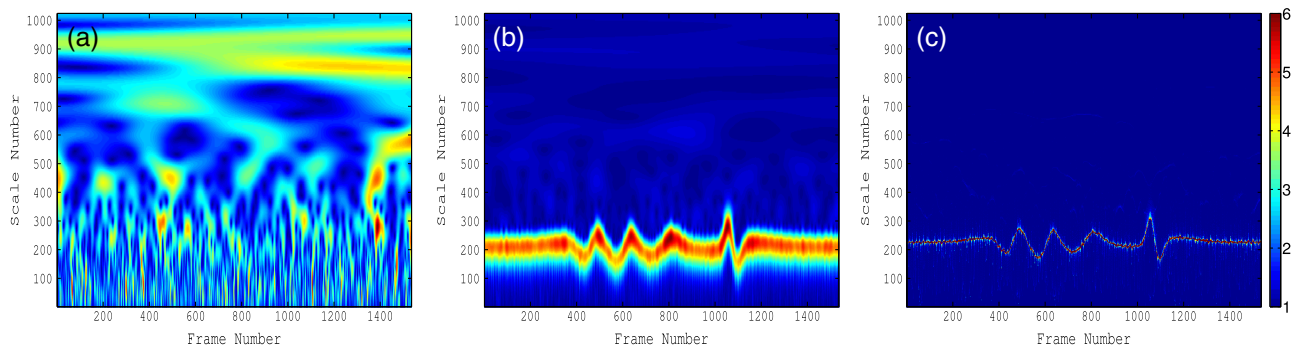
Fig. 4. (a) Scalogram obtained from the Morlet wavelet analysis of intensity in only one arm of the interferometer shown in Fig. 1, (b) the same scalogram in (a) for the signal difference by using both interferometric arms, and (c) synchrosqueezing algorithm applied to the case (b).
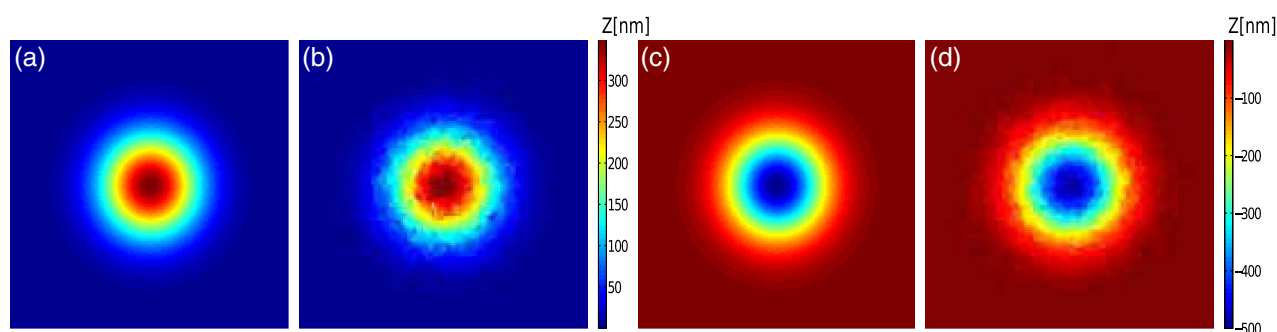

Fig. 5. Comparison of the displacement field corresponding to the spatial recovered phase difference between reference points given in Fig. 3: (a) and (c) ϕ_{AC} and ϕ_{BC} original phase difference, respectively; (b) and (d) ϕ_{AC} and ϕ_{BC} recovered phase difference, respectively.
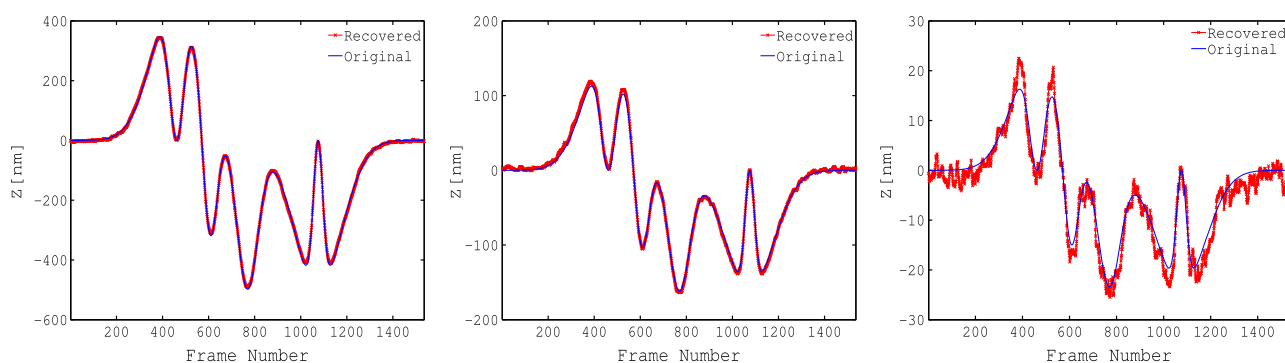

Fig. 6. Comparison between the original (blue) and recovered (red) temporal displacement fields corresponding to the pixels: (a) central (64,64), (b) medium (48,48), and border (37,37).

respectively. In this spatial phase recovery procedure, a conventional median filter was applied by using a 3×3 pixel window for typical disengage removal.

Finally, to highlight the obtained performance in the time domain when the proposed approach is used, Figs. 6(a), 6(b) and 6(c), respectively, compare the original and recovered temporal history of the displacement field corresponding to the spatial positions: central (64,64), medium (48,48), and border (37,37). The synchrosqueezing method reproduces the original phase quite well and it also can track the temporal evolution of low excursions imbedded in high levels of noise. From Figs. 5 and 6, it should be highlighted that the synchrosqueezing algorithm application can recover high and low values of the

phase when temporal speckle pattern interferometry signals are involved in the measurement system within noisy environments for a mean of speckle size of $s = 2$ pixels with an amplitude relation ratio of three orders of magnitude. We also tested the synchrosqueezing approach in several conditions and better performance is obtained for $s = 1$.

Below we offer a closer look at the obtained performance of the synchrosqueezing approach when a simultaneous $\pi/2$ phase-shifting heterodyne interferometer is used in temporal speckle pattern signals. We quantified the performance of the proposed approach by using a quality index $Q(t_n)$ calculated at each temporal frame. The spatial distortion of phase images between the original object phase ϕ_E
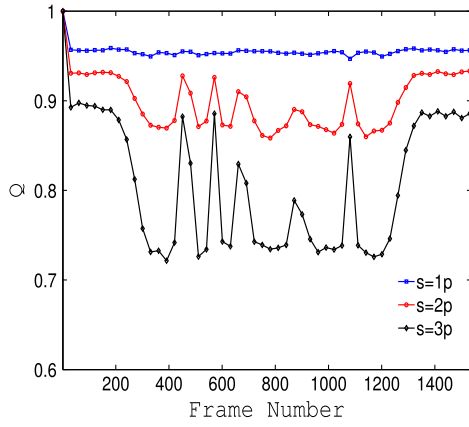
Fig. 7. Temporal evolution of the SSIM index Q with squares (blue), circles (red), and rhomboids (black) corresponding to $s = 1$, $s = 2$, and $s = 3$ pixels, respectively.

and the recovered phase ϕ_R is evaluated by means of the structural similarity (SSIM) index [11]. The distortion measured by the SSIM index is associated with the loss of correlation, undesired offset of mean phase, or alteration of standard deviation. The quality index is in the range of values $[-1, 1]$, where $Q = 1$ is satisfied for an exact phase retrieval. By using a sliding window approach for every temporal frame, we calculated a local index Q_L by means of the relation

$$Q_L = \frac{2(2\bar{\phi}_E\bar{\phi}_R + C_Q)(\sigma_{\phi_E\phi_R} + C_Q)}{(\bar{\phi}_E^2 + \bar{\phi}_R^2 + C_Q)(\sigma_{\phi_E}^2 + \sigma_{\phi_R}^2 + 2C_Q)}, \qquad (6)$$

where σ_{ϕ_E} and σ_{ϕ_R} are standard deviations of ϕ_E and ϕ_R, respectively; $\sigma_{\phi_E\phi_R}$ is the correlation coefficient between ϕ_E and ϕ_R; $\bar{\phi}_E$ and $\bar{\phi}_R$ are the means of both portions of the images; and C_Q is a small positive constant that avoids numerical instability for near zero sample means, variances and correlations. Note that the number of frame dependence is omitted for clarity. We obtained the SSIM index $Q(t)$ by calculating the average of all local index values Q_L for the defined constant $C_Q = 0.005$. By applying this quality measure to Fig. 5, we obtained the quality indexes

$Q = 0.80$ and $Q = 0.87$ for the recovered phases corresponding to Figs. 5(b) and 5(d), respectively.

These quality index values show a good correspondence with the original phase differences for the established noisy conditions. Observe the improved performance obtained by applying the synchrosqueezing transform. Furthermore, using the complete temporal history of the recovered phase values, Fig. 7 shows the temporal evolution of the SSIM index for the average speckle sizes of $s \in \{1, 2, 3\}$ pixels. Clearly, $s = 1$ pixel is the best working condition.

5. Experimental Results

Following Fig. 1, the light that travels along the test arm is reflected on the rough surface of a disc composed by a piezoelectric material, which is taken as the device under test. This DUT is imaged onto the sensor plane corresponding to each camera, CCD1 (Stingray F145B) and CCD2 (Stingray F146B), using a 100 mm focal length lens. The polarizations are separated by using a polarized beam splitter that redirects the different polarization components to each camera, which captures the same region of interest (ROI) of the sample. To align both cameras, we had to place them at the same optical distance from the DUT with their sensors perpendicular to the optical path and the same angle of rotation with respect to the horizontal plane.

Two cameras with the same resolution (1388×1008 pixels) and different sensor sizes (2/3 inches and 1/2 inches, respectively), are used in the experimental setup. Therefore, an integration procedure is implemented to match the size of the higher resolution into the lower resolution images corresponding to the elected ROI (36×130 pixels). Despite efforts made in alignment, some additional differences were detected and should be properly corrected. Because of the different pixel sizes of the two image sensors (6.45 μm and 4.65 μm for CCD1 and CCD2, respectively), each one has different quantum efficiency. Consequently, for the same incident intensity, the recorded intensities are different and the dynamic range of the smaller size pixel sensor is comparatively reduced. The left part of Fig. 8 compares the
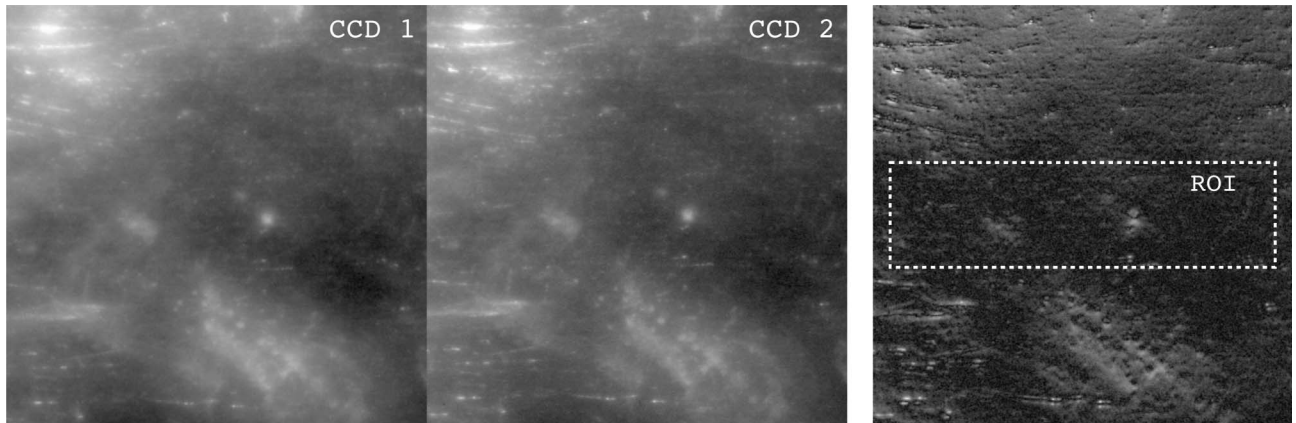

Fig. 8. Left: Acquired images corresponding to the surface of the DUT using white light illumination. Right: absolute difference corresponding to the intensities in each camera, CCD1 and CCD2.
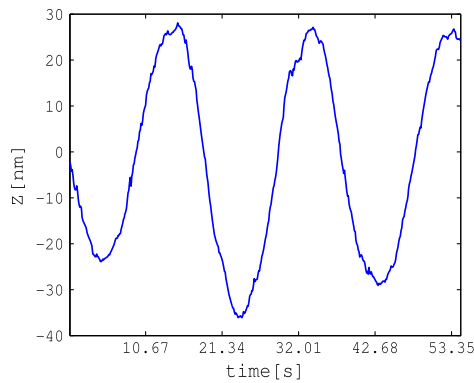
Fig. 9. Displacement of the central pixel in the selected ROI (36 × 130 pixels) depicted in Fig. 8.

acquired images corresponding to the surface of the DUT. To highlight the effects introduced by the additional differences obtained, the right part of Fig. 8 shows the absolute difference $\Delta(I) = |I_{CCD1} - I_{CCD2}|$ corresponding to the intensities I_{CCD1} and I_{CCD2} in each camera. Satisfactory results were obtained with the application of an image registration algorithm [12] to ensure the suitably spatial match of both captures in the selected ROI. Interested readers also can implement a script based on MATLAB built in functions: imregconfig and imregister.

Since the dynamic interferometric measurement relies on the simultaneous acquisition of two $\pi/2$ rad out of phase images, both cameras are actuated by a common trigger signal and have equal exposure time. In addition, we excited the piezoelectrically

driven mirror with a 12-level stair-step signal with smoothed edges that produces $\lambda/12$ phase shifts in the reference arm synchronized with the trigger signal. The stair-step signal has modified excursions to compensate the piezoelectric actuator nonlinearities. A low frequency and voltage sinusoidal signal (40 mHz, 10 V Offset and 300 mV Vpp) was applied to the DUT to produce the out-of-plane nanometric displacements. Although we captured a sequence of 640 frames, some data was removed to take into consideration border effects, so we analyzed 512 effective temporal frames. This data included several carrier phase shift cycles corresponding to 11311 nm for 2.5 displacement periods of the DUT.

Figure 9 shows the displacement obtained for the central pixel in the selected ROI depicted in Fig. 8. Figures 10(a), 10(b), and 10(c) illustrate the obtained results for the specific frame numbers 226, 274, and 325, respectively. Figures 10(a) and 10(c) show the negative and positive maximum excursions, respectively, and Fig. 10(b) depicts the zero crossing transition.

The performance obtained for the simultaneous $\pi/2$ phase-shifting heterodyne interferometer assisted with the synchrosqueezing transform method is also compared by generating out-of-plane displacements by means of a nanopositioning transducer (PI Z-Stage model P-611.Z0). In this case, the DUT is replaced by the Z-Stage running excursions in the interval ±10 nm following a triangular signal. Figure 11(a) illustrates the obtained temporal evolution corresponding to the central pixel of a mirror
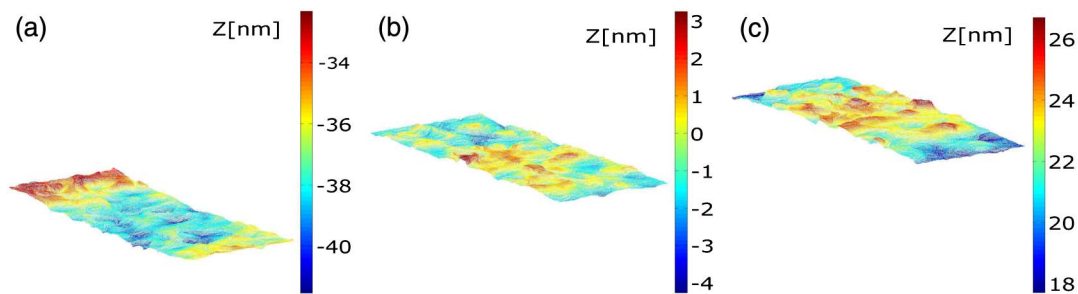

Fig. 10. Spatiotemporal displacement field corresponding to the ROI (36 × 130 pixels) shown in Fig. 8 for the frame numbers: 226 (a); 274 (b); and 325 (c).
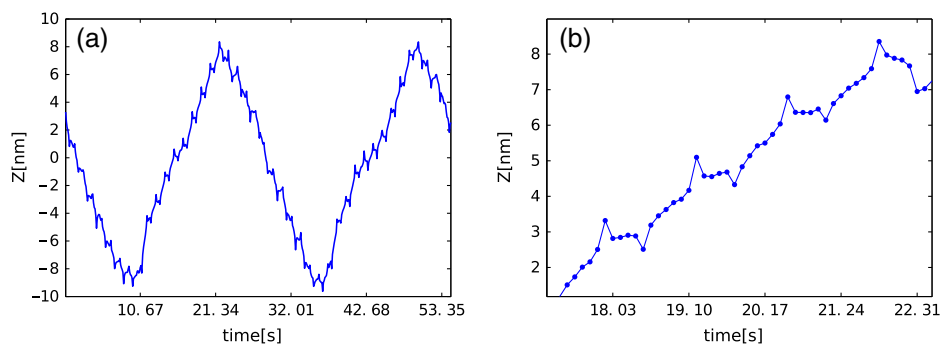

Fig. 11. (a) temporal evolution of the central pixel corresponding to a mirror mounted over the mechanical head of the Z-Stage and (b) details of the systematic fluctuations shown in (a).

mounted over the mechanical head of the Z-Stage. Note that the systematic fluctuations in the movement of the piezo-electrically driven mirror due to the presence of nonlinearities are well detected. In Fig. 11(b) these fluctuations are zoomed. Each dot in the picture corresponds to a specific measurement.

6. Conclusions

We evaluated a method for amplitude and phase retrieval in simultaneous $\pi/2$ phase-shifting heterodyne interferometry to be used in dynamic micro- and nanometric measurements. The proposed optical setup admits the introduction of a temporal carrier and simultaneously verifies the two-beam interferometry equation for each intensity signal that are $\pi/2$ rad out of phase (quadrature). The application of this optical setup allows the use of differential working conditions. Therefore, the measurement system can recover very low phase value excursions. We have shown that the associated representation of the differential signal in the wavelet domain is still too vague to obtain good results and consequently the application of the ridge extraction procedure failed. The synchrosqueezing transform is applied to obtain a more clear time-scale representation and therefore a better phase retrieval process is obtained. We illustrate the experimental phase recovery process by analyzing temporal speckle pattern interferometric signals and obtain valuable results. In addition, the sensibility of the measurement system is experimentally evaluated by detecting the systematic fluctuations in the movement of a piezo-electrically driven mirror due to the presence of nonlinearities. Finally, we would like to highlight that the alignment procedures are laborious. In this work we have shown that the application of regularization techniques favors the accuracy of the obtained results when the CCD sensors are sightly dissimilar. We will present new insights and an exhausted evaluation of this phase retrieval method in a future paper.

References

1. W. Osten, ed., *Optical Inspection of Microsystems* (CRC, 2007).
2. P. K. Rastogi, ed., *Digital Speckle Pattern Interferometry and Related Techniques* (Wiley, 2001).
3. A. Federico and G. H. Kaufmann, "Phase evaluation in temporal speckle pattern interferometry using time-frequency approaches," in *Advances in Speckle Metrology and Related Techniques*, G. H. Kaufmann, ed. (Wiley, 2011), Chap. 4.
4. P. Jacquot, "Speckle interferometry: a review of the principal methods in use for experimental mechanics applications," Strain **44**, 57–69 (2008).
5. B. Deutsch, R. Beams, and L. Novotny, "Nanoparticle detection using dual-phase interferometry," Appl. Opt. **49**, 4921–4925 (2010).
6. D. Malacara, ed., *Optical Shop Testing* (Wiley, 2007).
7. F. Auger, P. Flandrin, Y.-T. Lin, S. McLaughlin, S. Meignen, T. Oberlin, and H.-T. Wu, "Time-frequency reassignment and synchrosqueezing: an overview," IEEE Signal Process. Mag. **30**(6), 32–41 (2013).
8. I. Daubechies, J. Lu, and H. Wu, "Synchrosqueezed wavelet transforms: an empirical mode decomposition-like tool," Appl. Comput. Harmon. Anal. **30**, 243–261 (2011).
9. G. Thakur, E. Brevdo, N. S. Fučkar, and H. Wu, "The synchrosqueezing algorithm for time-varying spectral analysis: robustness properties and new paleoclimate applications," Signal Process. **93**, 1079–1094 (2013).
10. S. Equis and P. Jacquot, "Simulation of speckle complex amplitude: advocating the linear model," Proc. SPIE **6341**, 381–386 (2006).
11. Z. Wang, A. Bovik, H. Sheikh, and E. Simoncelli, "Image quality assessment: from error visibility to structural similarity," IEEE Trans. Image Process. **13**, 600–612 (2004).
12. D. Kroon and C. H. Slump, "MRI modality transformation in demon registration," in *IEEE International Symposium on Biomedical Imaging: From Nano to Macro*, Boston, MA, 28 June 2009 (IEEE, 2009), pp. 963–966.